

Fig. 15.1. Scattering of a plane wave incident from the left along the z direction by an attractive potential. The potential is confined to region $r < d$ indicated by the small half-circle. Shown are the real part, the imaginary part, and the absolute square of the wave function $\varphi_k^{(+)}$. The figure corresponds exactly to the situation of Figure 12.1, except for the change $V_0 \rightarrow -V_0$ in the scattering potential.

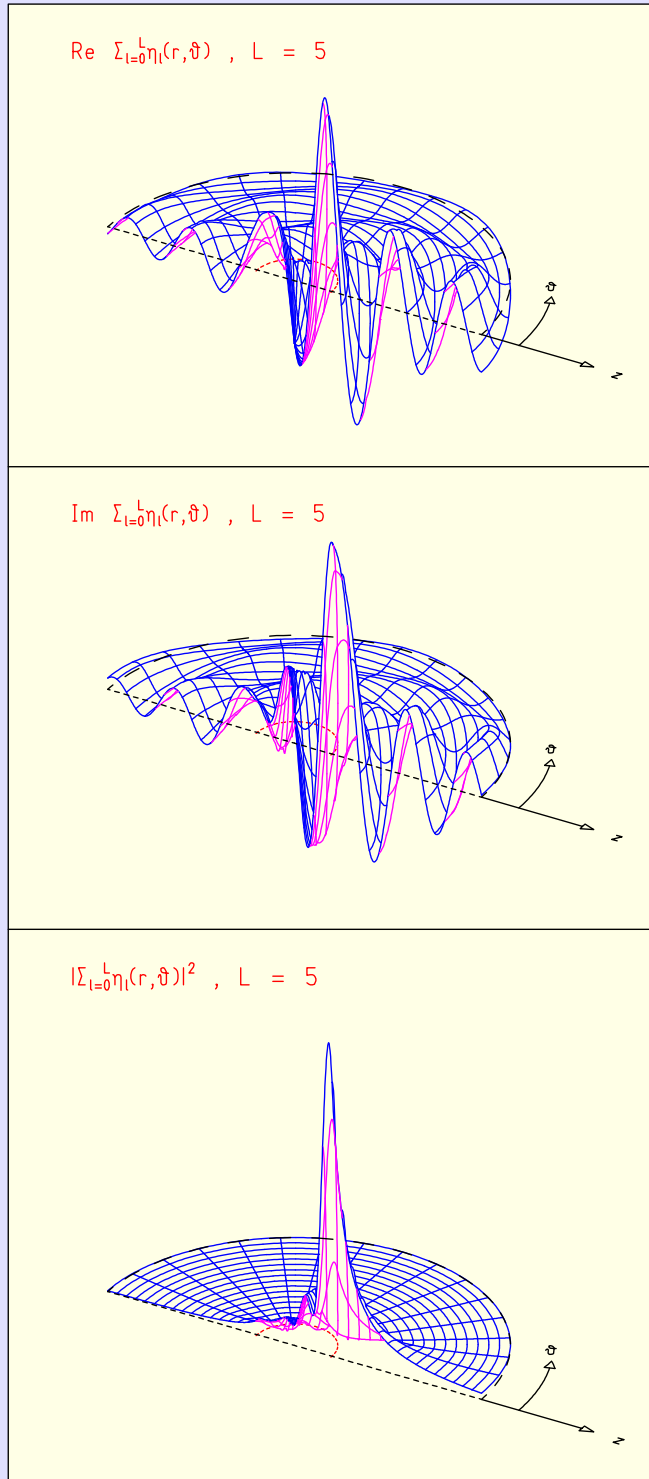


Fig. 15.2. Real part, imaginary part, and absolute square of the scattered spherical wave η_k resulting from the scattering of a plane wave by an attractive potential, as shown in Figure 15.1.

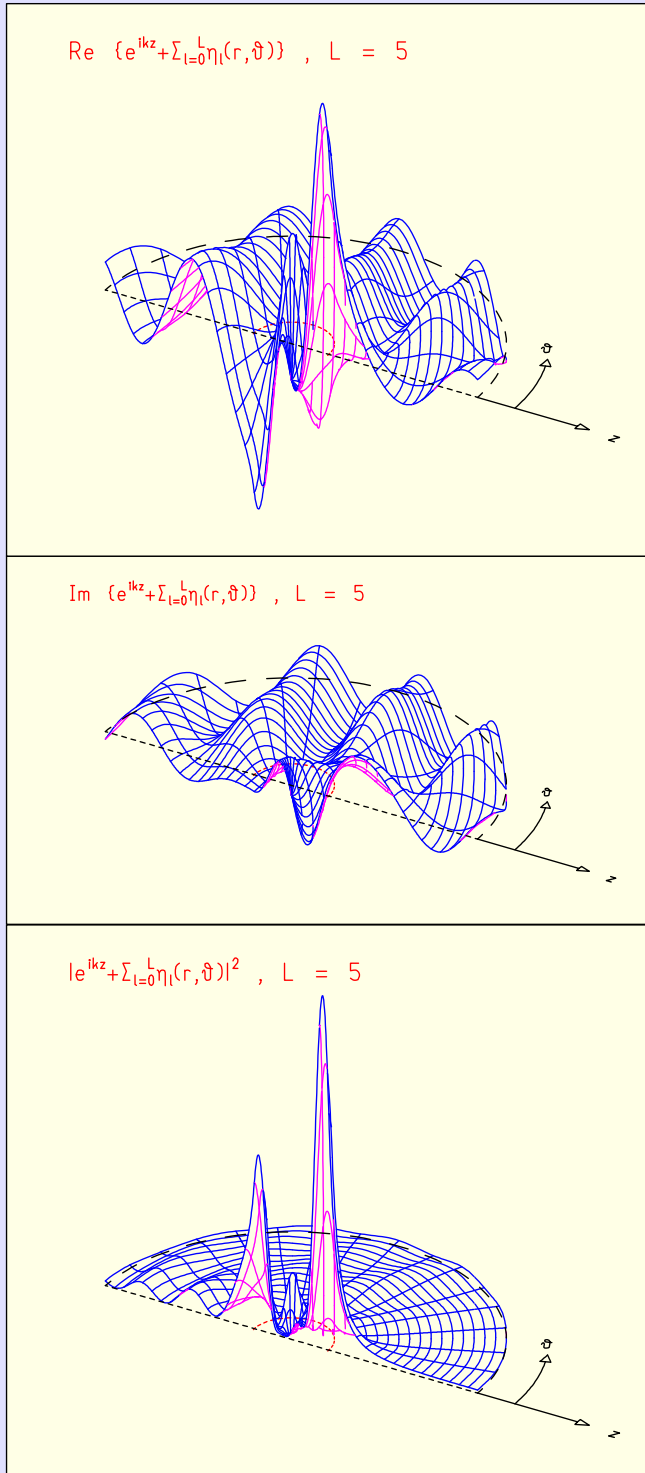


Fig. 15.3. Real part, imaginary part, and absolute square of the wave function $\varphi_{\mathbf{k}}^{(+)}$ for the scattering of a plane wave by an attractive potential as given in Figure 15.1, but for a resonance energy $E = E_{\text{res}}$ of the wave.

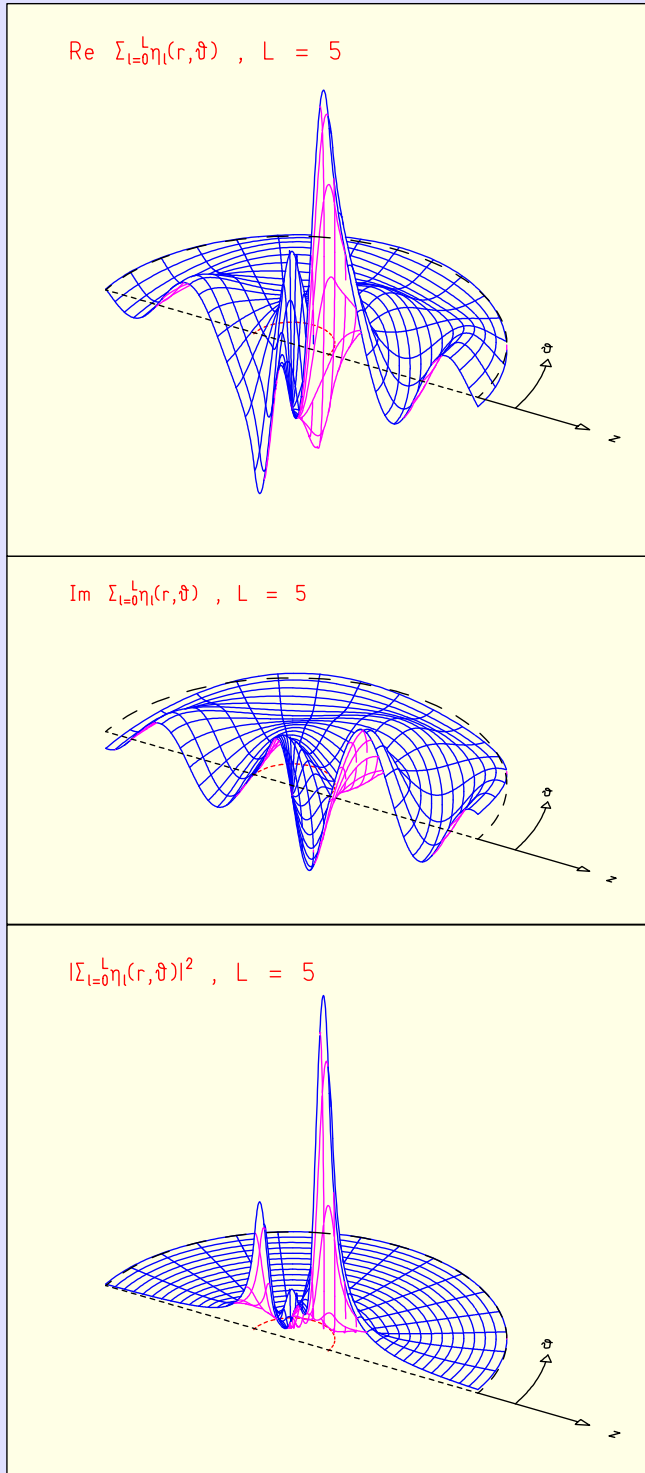


Fig. 15.4. Real part, imaginary part, and absolute square of the scattered spherical wave η_k resulting from the scattering of a plane wave of resonance energy $E = E_{\text{res}}$ by the same attractive potential as in Figure 15.3.

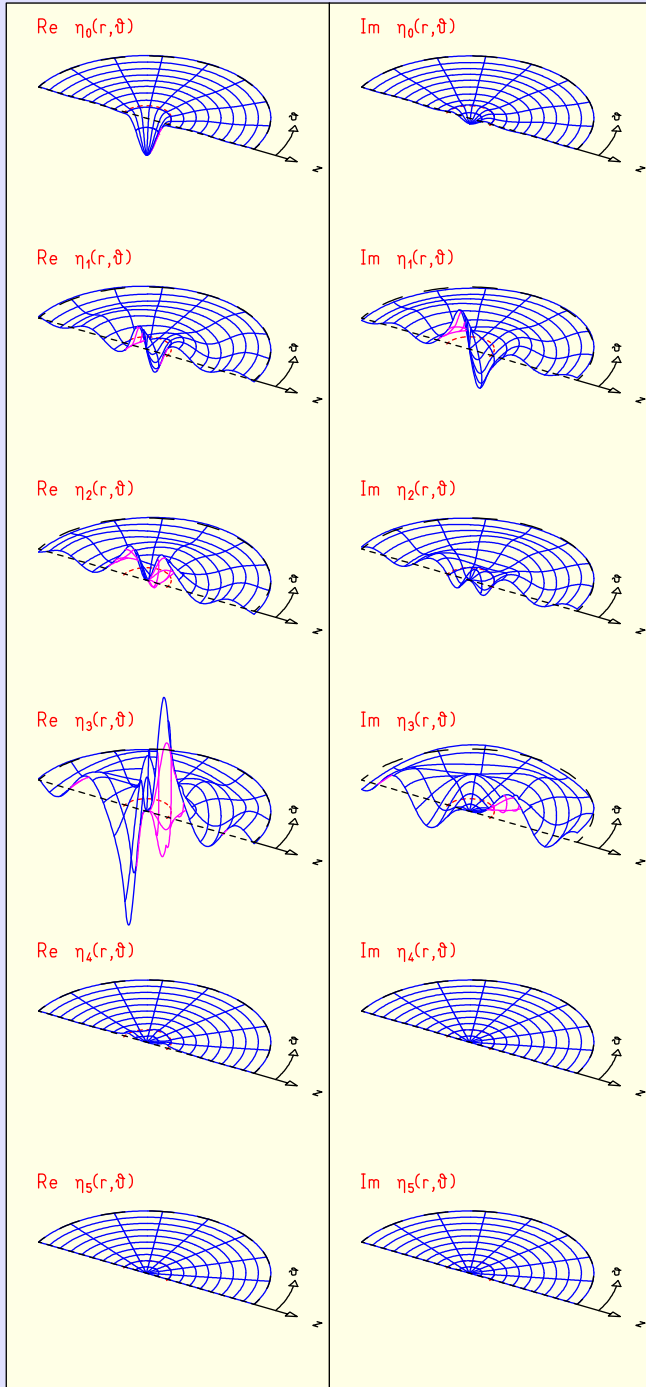


Fig. 15.5. Real and imaginary parts of the scattered partial waves η_ℓ resulting from the scattering of a plane wave of resonance energy $E = E_{\text{res}}$ by the attractive potential as in Figures 15.3 and 15.4. The resonance is in the partial wave for $\ell = 3$.

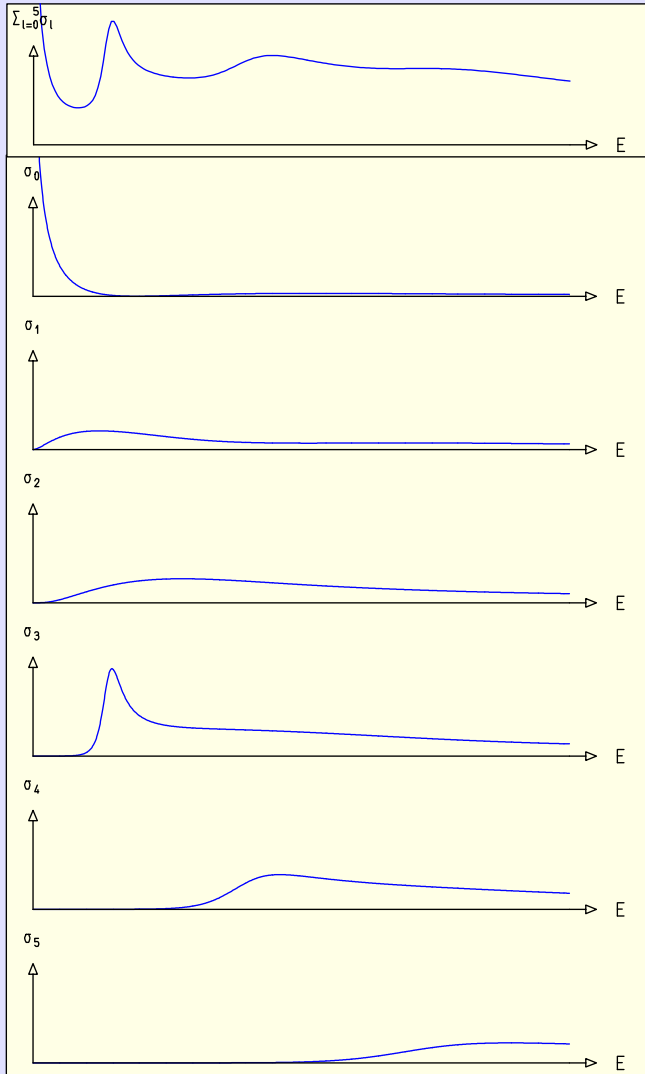


Fig. 15.6. The partial cross sections $\sigma_\ell(E)$ and the total cross section $\sigma_{\text{tot}}(E)$ approximated by the sum over the first few partial cross sections for the scattering of a plane wave of energy E by the attractive potential used in Figures 15.1 through 15.5. For resonant energy $E = E_{\text{res}}$ there is a sharp maximum in σ_3 which is reflected in σ_{tot} approximated by the sum over the first six partial cross sections and shown in the top diagram of the figure.

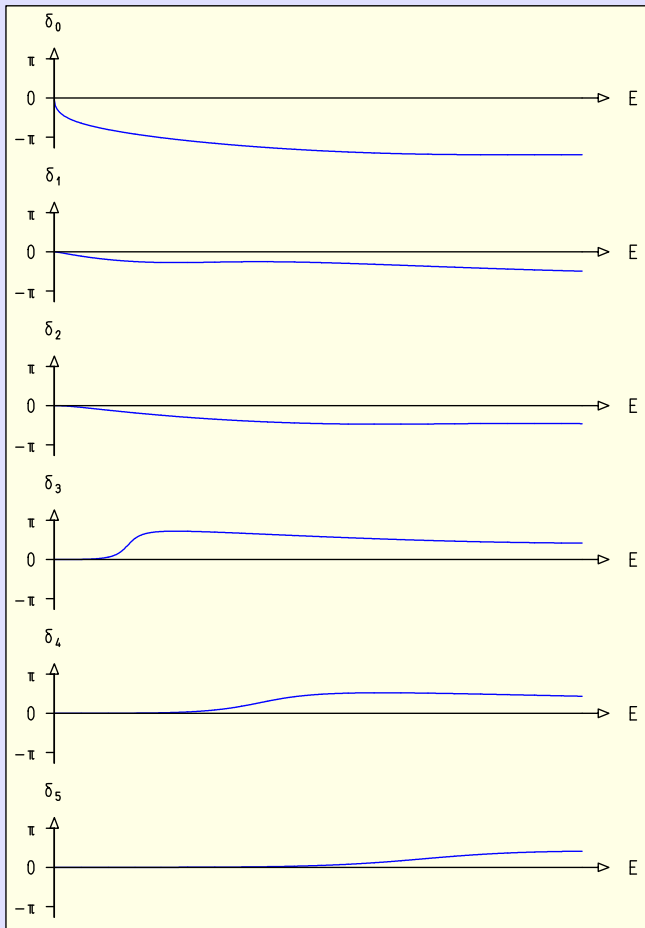


Fig. 15.7. The phase shifts $\delta_\ell(E)$ for the situation of Figure 15.6. For $E = 0$ we put $\delta_\ell(0) = 0$. All phase shifts except δ_3 vary only slowly with energy. Near $E = E_{\text{res}}$ the phase shift $\delta_3(E)$ rises sharply, passing through $\delta_3(E = E_{\text{res}}) = \pi/2$, see also the bottom right diagram in Figure 15.8.

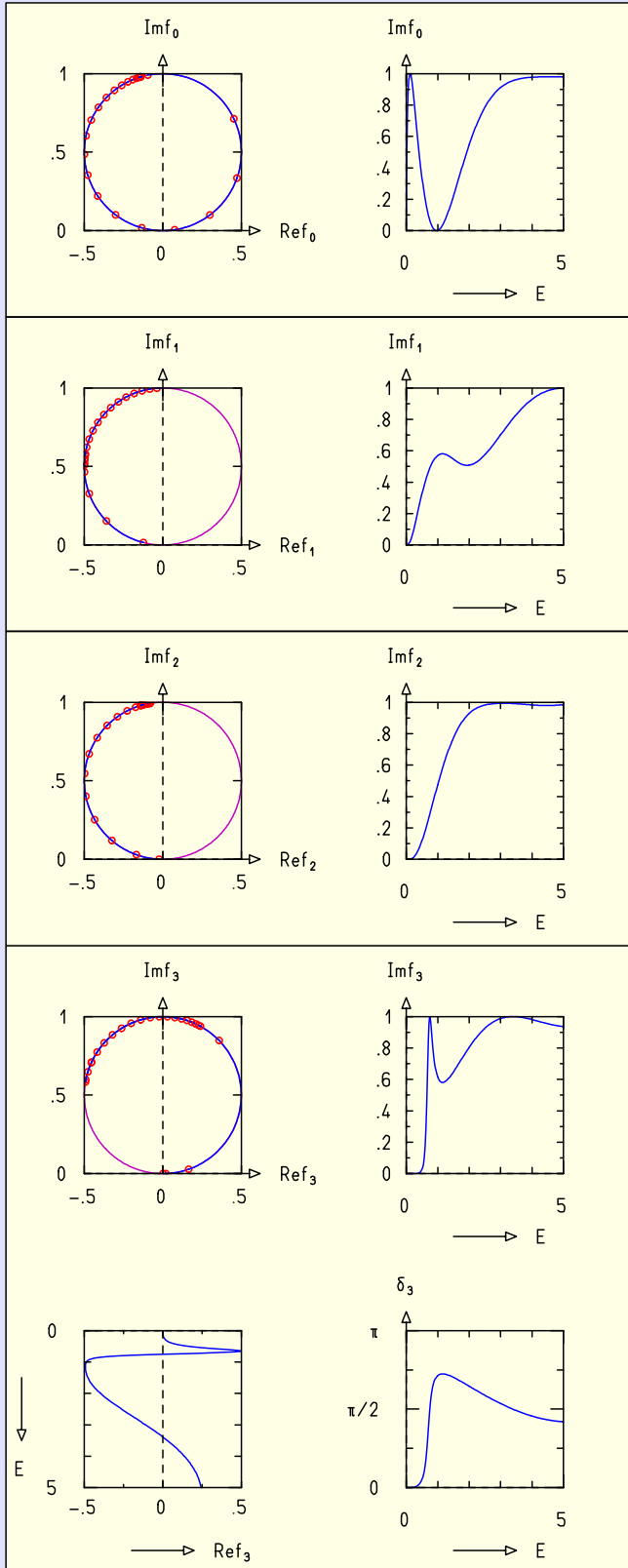


Fig. 15.8. Argand diagrams, that is, diagrams of the energy dependence of the complex partial scattering amplitudes $f_\ell(E)$, for the scattering of a plane wave of energy E by the attractive potential used in Figures 15.1 through 15.7 for $\ell = 0, 1, 2, 3$. The amplitude f_ℓ moves on a circle in the complex plane. Small circles are placed on the circle at points equidistant in energy. For the nonresonant partial waves, $\ell = 0, 1, 2$, only the Argand diagram itself and its projection on the $\text{Im} f_\ell, E$ plane are shown. The function $\text{Im} f_\ell(E)$ is closely related to the partial cross section $\sigma_\ell(E)$. For resonant wave $\ell = 3$ both $\text{Im} f_\ell(E)$ and $\text{Re} f_\ell(E)$ projections and the phase shift $\delta_3(E)$ are shown. Near resonance energy $E = E_{\text{res}}$ the partial scattering amplitude $f_3(E)$ performs a swift counterclockwise motion through point $(0, 1)$ in the complex plane, giving rise to (1) the pronounced maximum in $\text{Im} f_3(E_{\text{res}})$, (2) the steep drop of $\text{Re} f_3(E)$ through $\text{Re} f_3(E_{\text{res}}) = 0$, and (3) the sharp rise of $\delta_3(E)$ through $\delta_3(E_{\text{res}}) = \pi/2$.

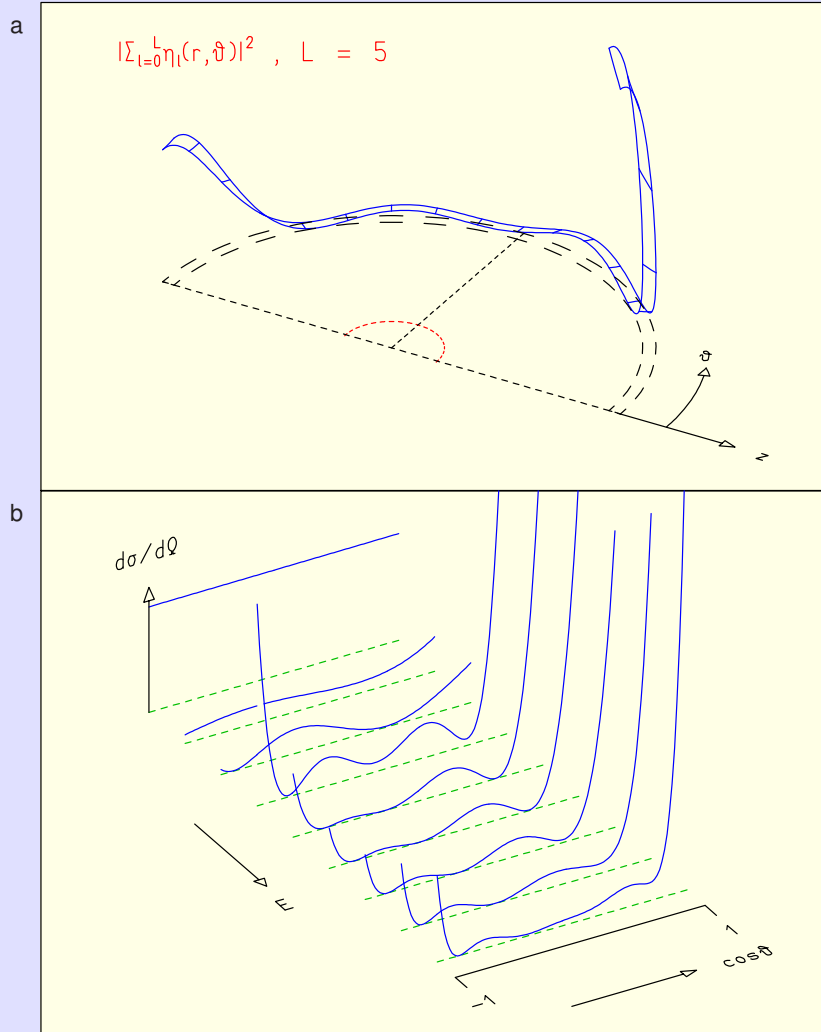


Fig. 15.9. (a) Intensity of the scattered spherical wave resulting from the scattering of a plane wave incident in the z direction onto an attractive potential restricted to a small region $r < d$, indicated by the small dashed half-circle. The intensity far outside the potential region is a function of the scattering angle ϑ . The energy of the incident wave is the resonance energy $E = E_{\text{res}}$. (b) Energy dependence of the differential scattering cross section $d\sigma/d\Omega$ shown over a linear scale in $\cos \vartheta$. The differential cross section is constant in $\cos \vartheta$, indicating isotropic scattering, for $E \approx 0$ (background). At resonance energy $E = E_{\text{res}}$ (fourth line from the back) it is given approximately by the square of the Legendre polynomial $P_3(\cos \vartheta)$, since the partial scattering amplitude f_3 dominates the cross section.

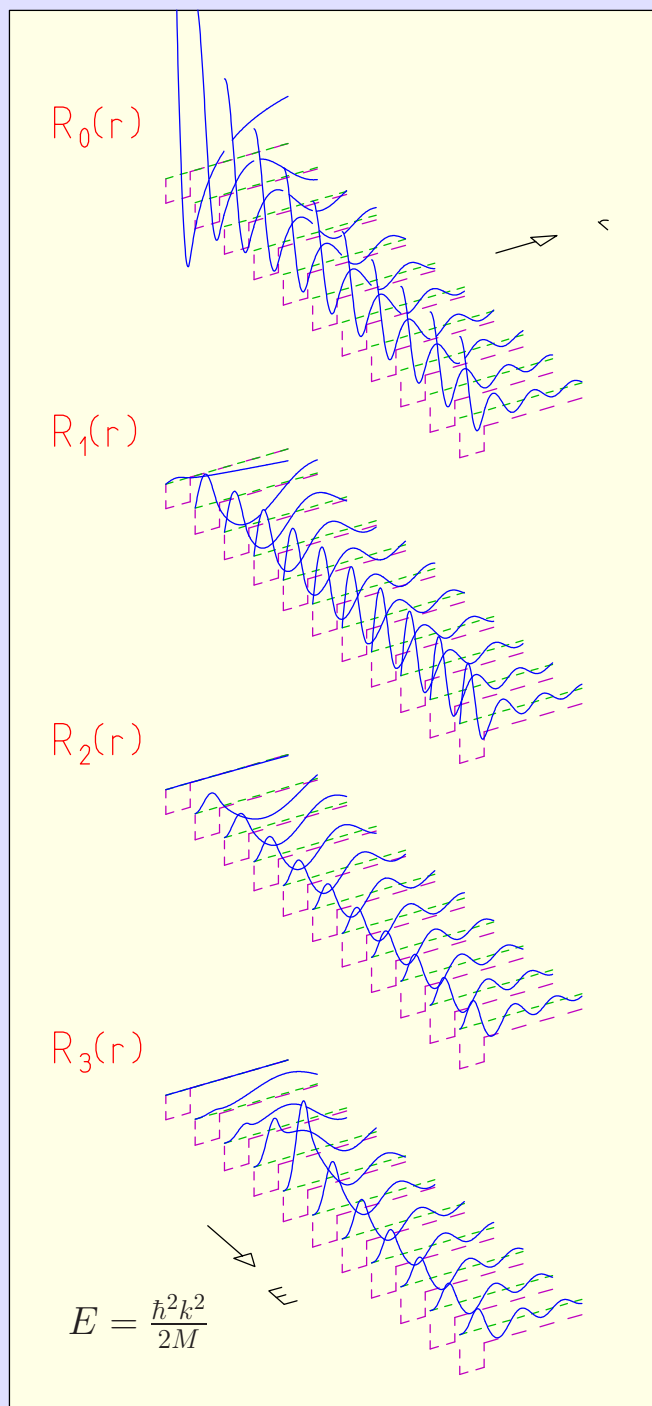


Fig. 15.10. Energy dependence of the radial wave function $R_\ell(k, r)$ for scattering by an attractive square-well potential. The form of the potential is indicated by the long-dash line, the wave energy by the short-dash line, which also serves as zero line for the wave function. Whereas R_0 , R_1 , and R_2 change very little within the potential region, near the energy E_{res} the wave function R_3 of the resonant partial wave develops a very pronounced maximum. Outside the potential region all wave functions show trivial shortening of the wavelength with growing energy.

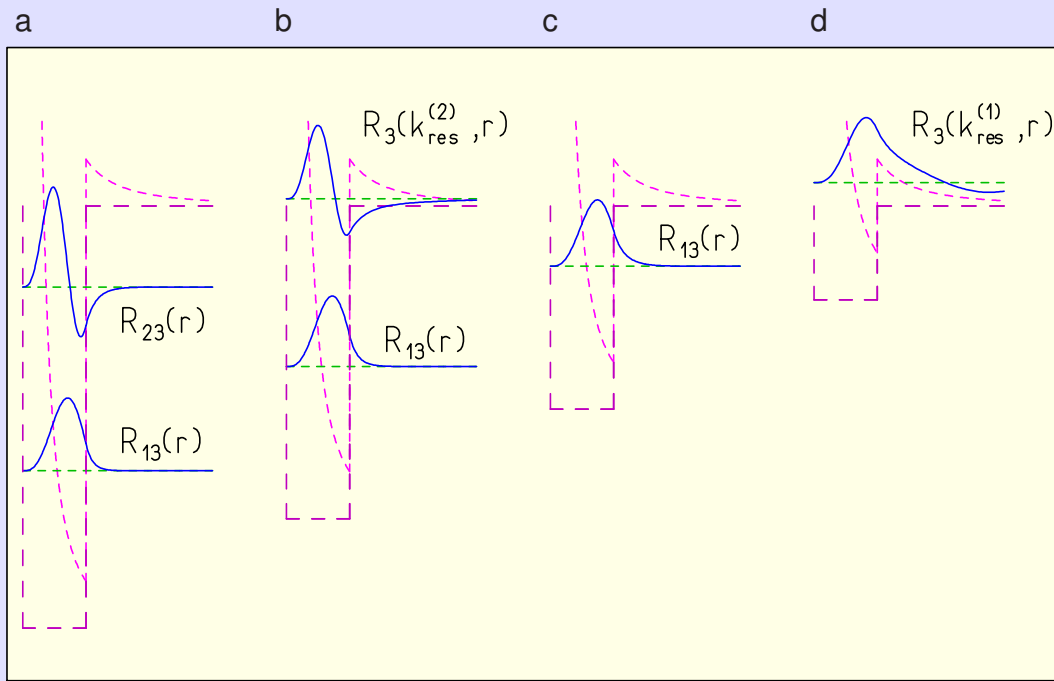


Fig. 15.11. Bound states and resonances of an attractive square-well potential for angular-momentum quantum number $\ell = 3$. The potential wells have constant fixed widths but different depths. The potential $V(r)$ is shown as a long-dash line. The effective potential is also shown. (a) For a rather deep potential well there are two bound states with negative energies indicated by the horizontal short-dash lines. The lower bound state has no radial nodes; the second has one node. (b) A somewhat shallower well has only one bound state but it does have a resonance. The resonance energy corresponds to the horizontal line of positive energy. The radial wave function $R_3(k_{\text{res}}^{(2)}, r)$ has one node in the potential region, just as the second bound state in part a has. (c) This potential well has only one bound state. (d) The bound state in part c now reappears as a resonance. Its wave function is $R_3(k_{\text{res}}^{(1)}, r)$. The resonance is the same as that in Figures 15.3 through 15.10.

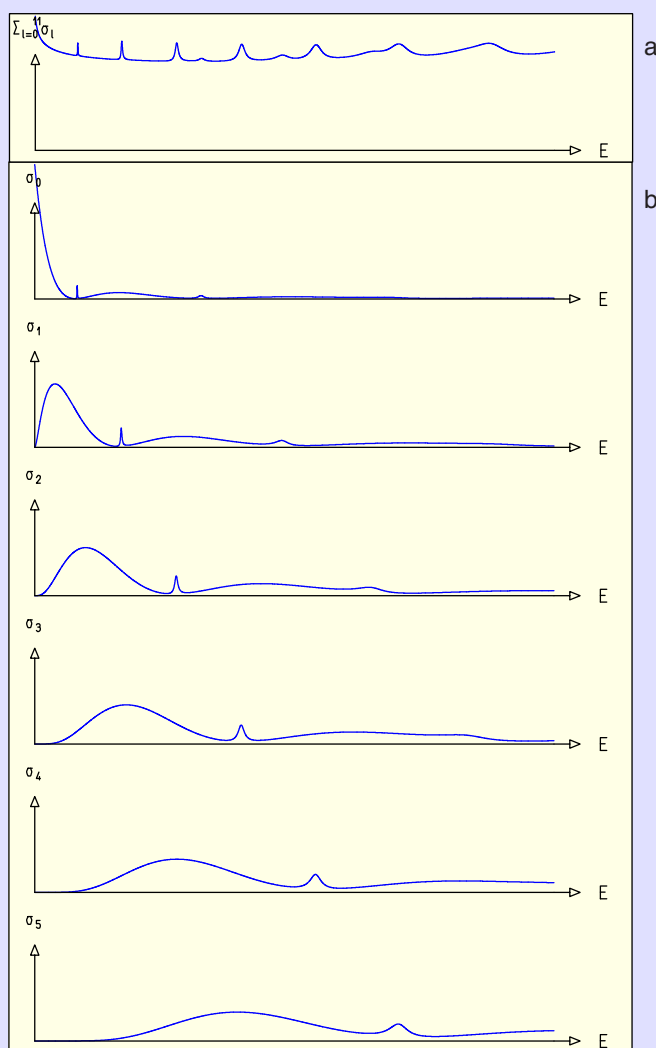


Fig. 15.12. Energy dependence of the partial cross sections $\sigma_\ell(E)$ and of the total cross section $\sigma_{\text{tot}}(E)$, which is approximated by the sum over the first few partial cross sections. Resonances for the different partial waves are visible as maxima in σ_ℓ and σ_{tot} . The maxima are rather sharp for the first resonance and broader for the second. The resonances shift systematically to higher energies as angular-momentum quantum number ℓ increases. The energy ranges from $E = 0$ to $E = 2V_0$.

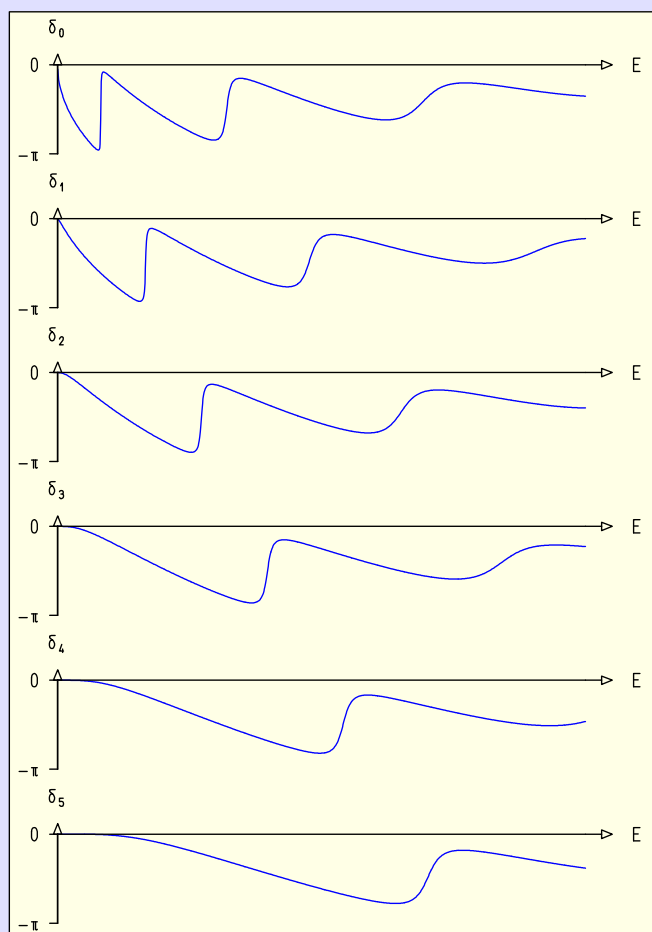


Fig. 15.13. Energy dependence of the phase shifts $\delta_\ell(E)$. At a resonance energy the corresponding phase shift rises steeply and passes through $-\pi/2$. See also Figure 15.14. The energy ranges from $E = 0$ to $E = 2V_0$.

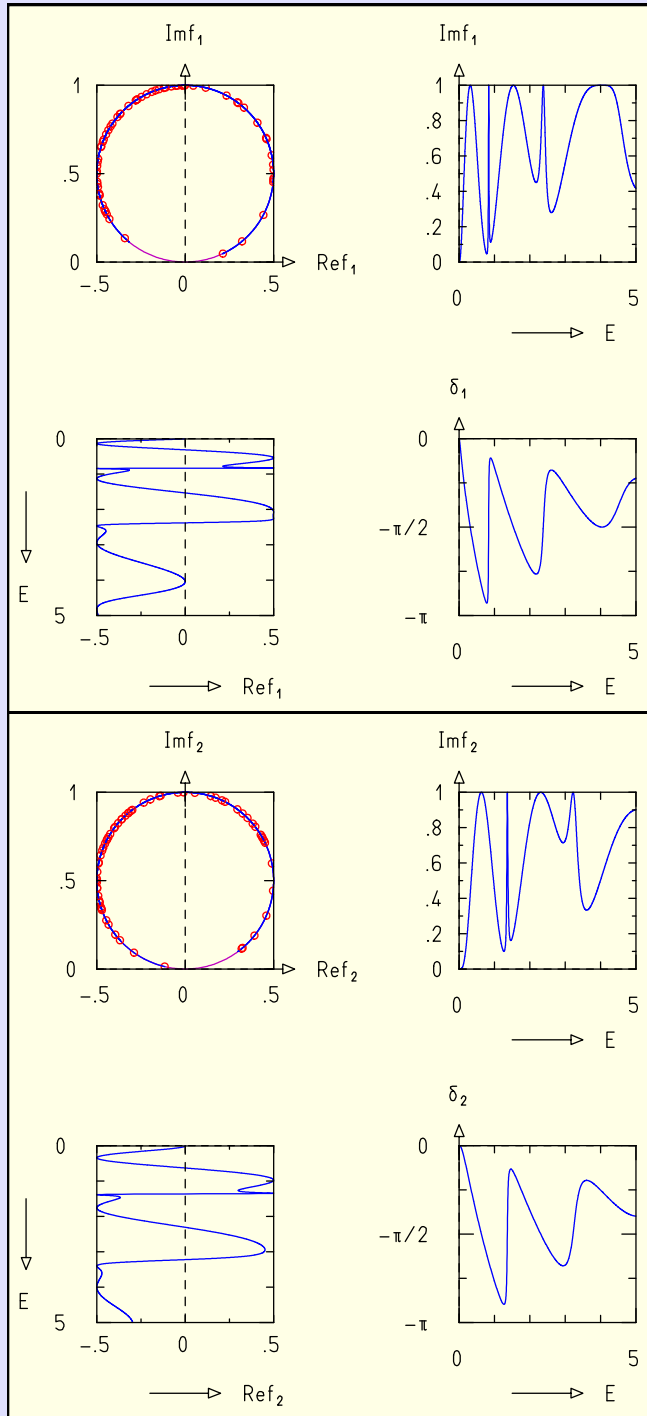


Fig. 15.14. Argand diagrams for the complex partial scattering amplitudes $f_1(E)$ and $f_2(E)$ for scattering by a repulsive shell. As in Figures 15.12 and 15.13, the energy ranges from $E = 0$ to $E = 2V_0$. The resonances have a swift counterclockwise motion of f_ℓ through the point $(0, 1)$ in the complex plane, and the characteristic resonance patterns in $\text{Im} f_\ell(E)$, $\text{Re} f_\ell(E)$, and $\delta_\ell(E)$ already familiar from Figure 15.8 (bottom). Because of the shell structure of the potential, there are now more resonances.

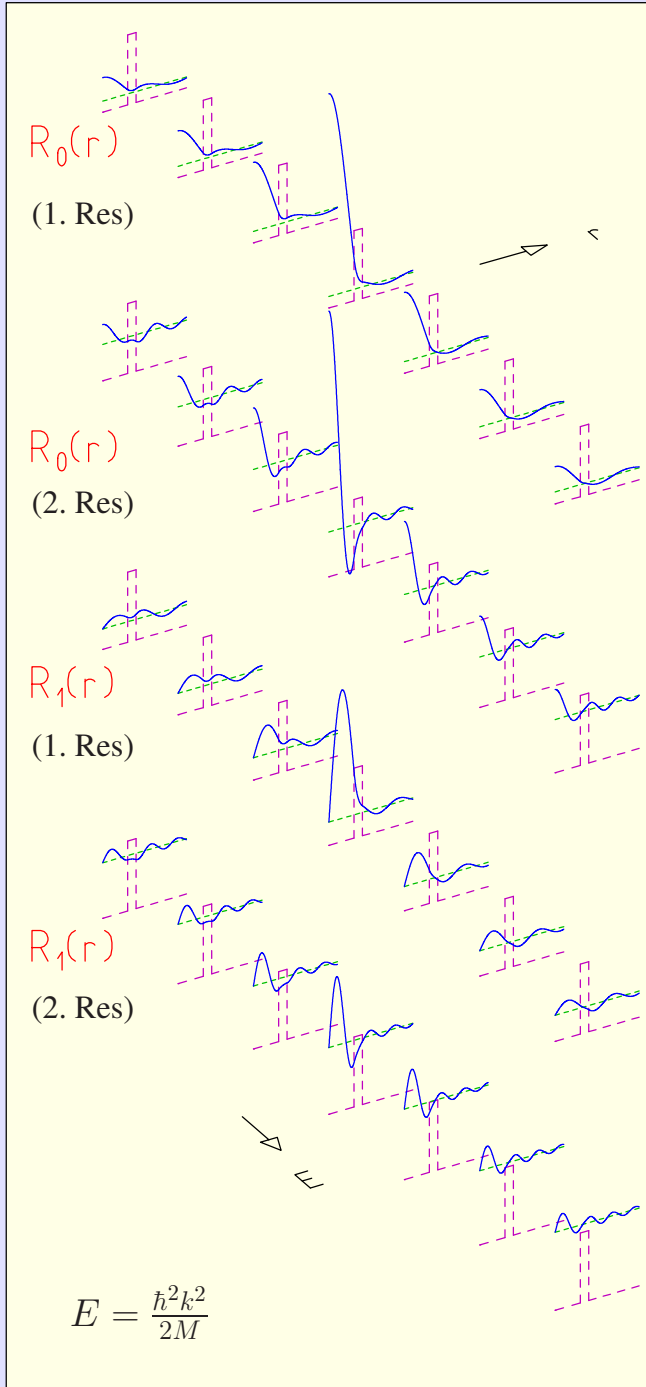


Fig. 15.15. Energy dependence of the radial wave functions $R_\ell(k, r)$ within restricted energy intervals surrounding the resonances in $\ell = 0$ and in $\ell = 1$ for scattering by a repulsive shell. The form $V(r)$ of the potential is indicated by the long-dash line, the energy E of the wave by the short-dash line. The middle diagram of each series corresponds to the resonance energy. The wave functions $R_\ell(k_{\text{res}}, r)$ shown in these middle diagrams display no node and one node inside the shell for the first and second resonance, respectively.

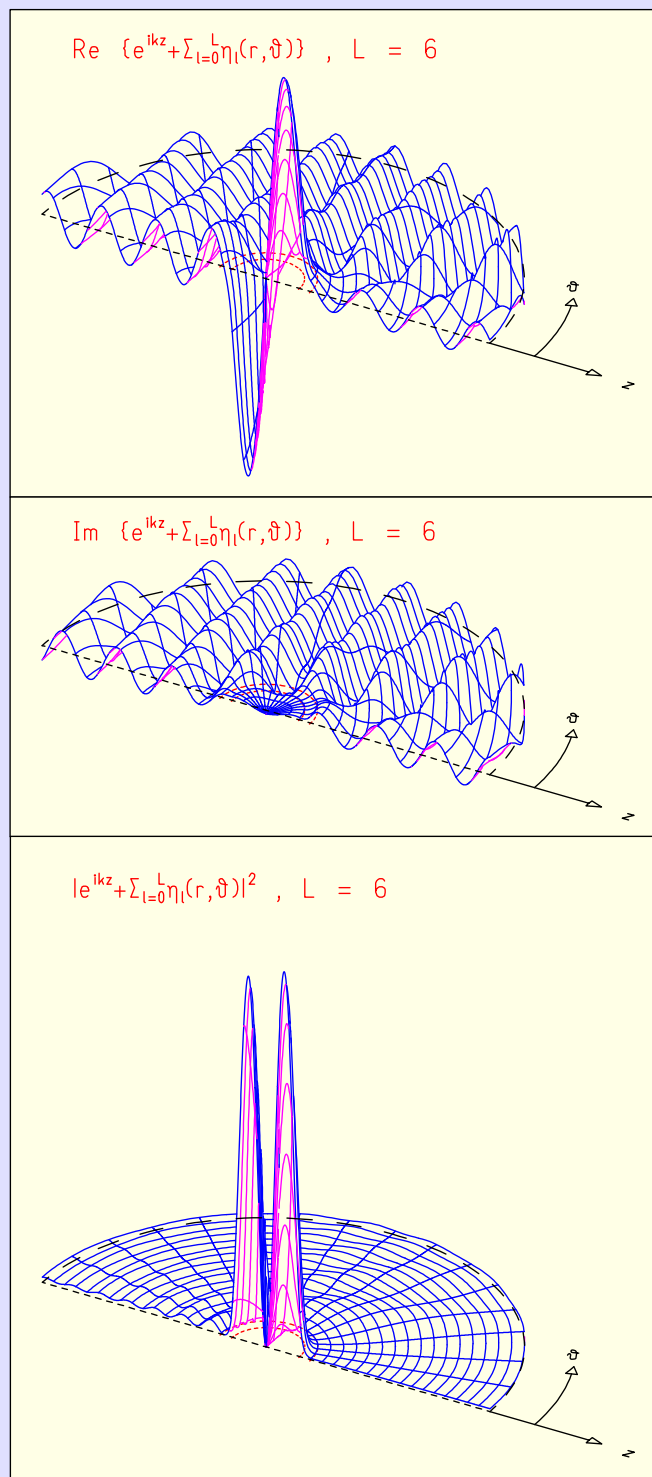


Fig. 15.16. Wave functions $\varphi_{\mathbf{k}}^{(+)}$ for the scattering of a plane wave incident along the z direction by a repulsive shell. The energy is that of the first resonance in partial wave $\ell = 1$. The two half-circles near the center indicate the inner and outer boundaries of the spherical potential shell.

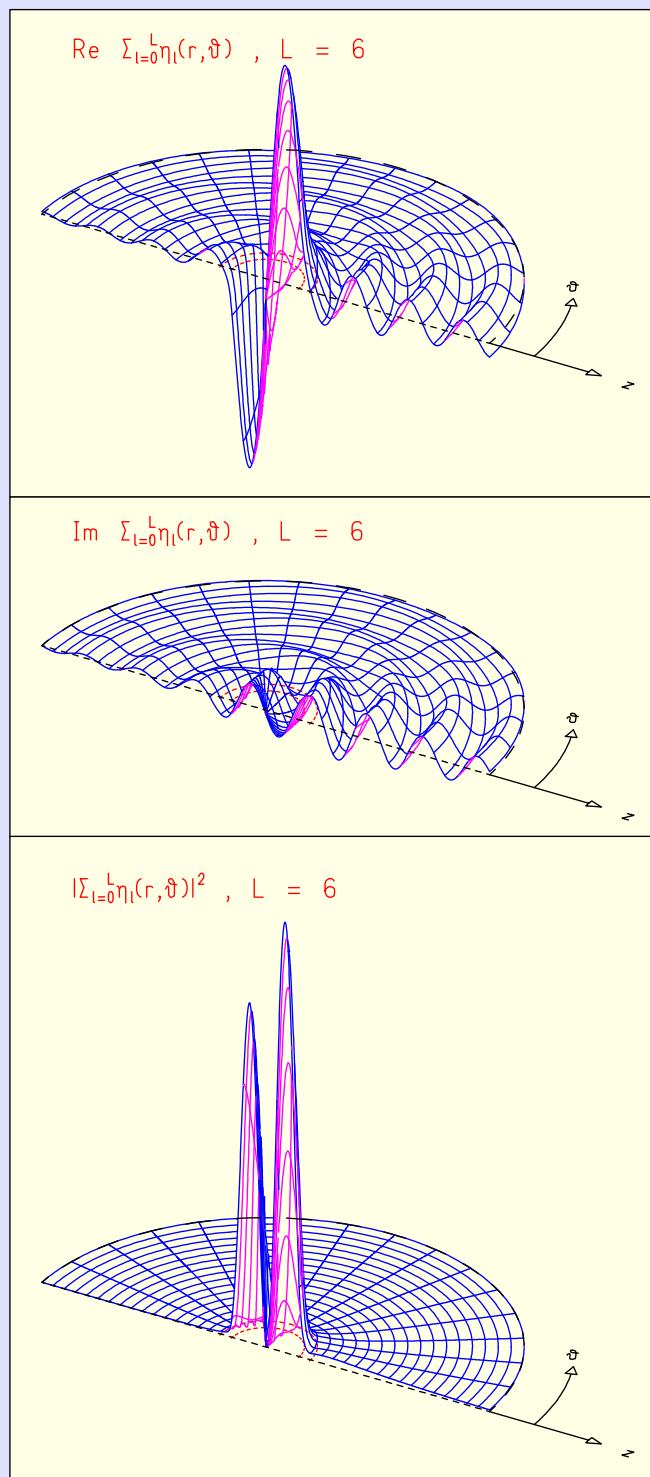


Fig. 15.17. The scattered spherical wave η_k resulting from the scattering of a plane wave incident along the z direction by a repulsive shell. The energy is that of the first resonance in partial wave $\ell = 1$.

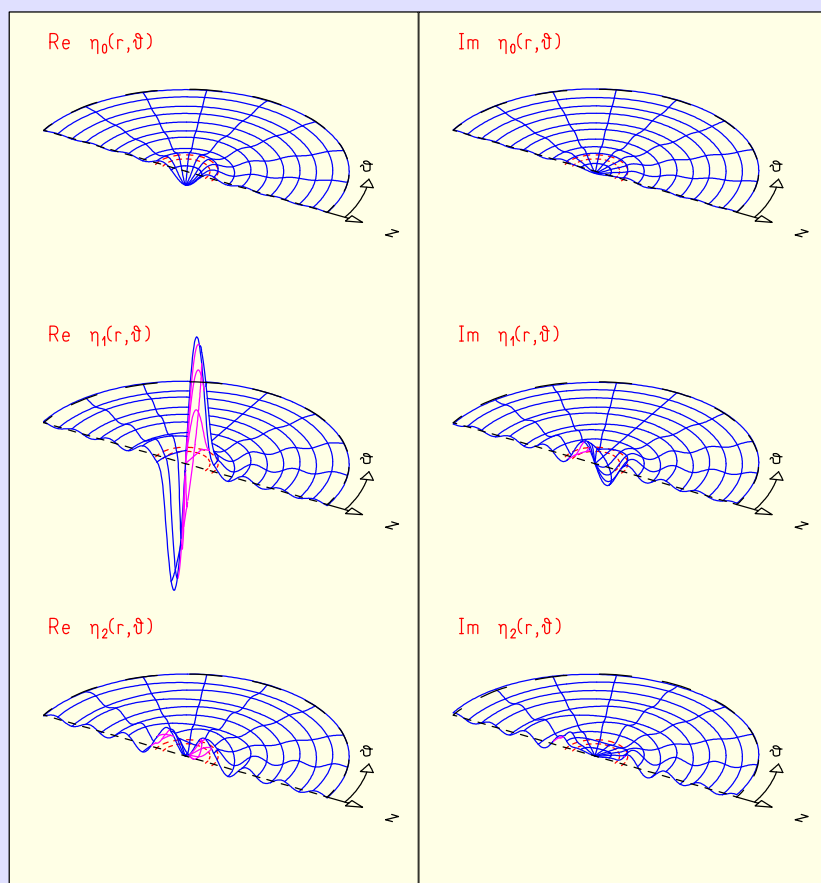


Fig. 15.18. Scattered partial waves η_ℓ , $\ell = 0, 1, 2$, resulting from the scattering of a plane wave incident along the z direction by a repulsive shell. The partial wave η_1 has its first resonance at this particular energy of the incident plane wave.

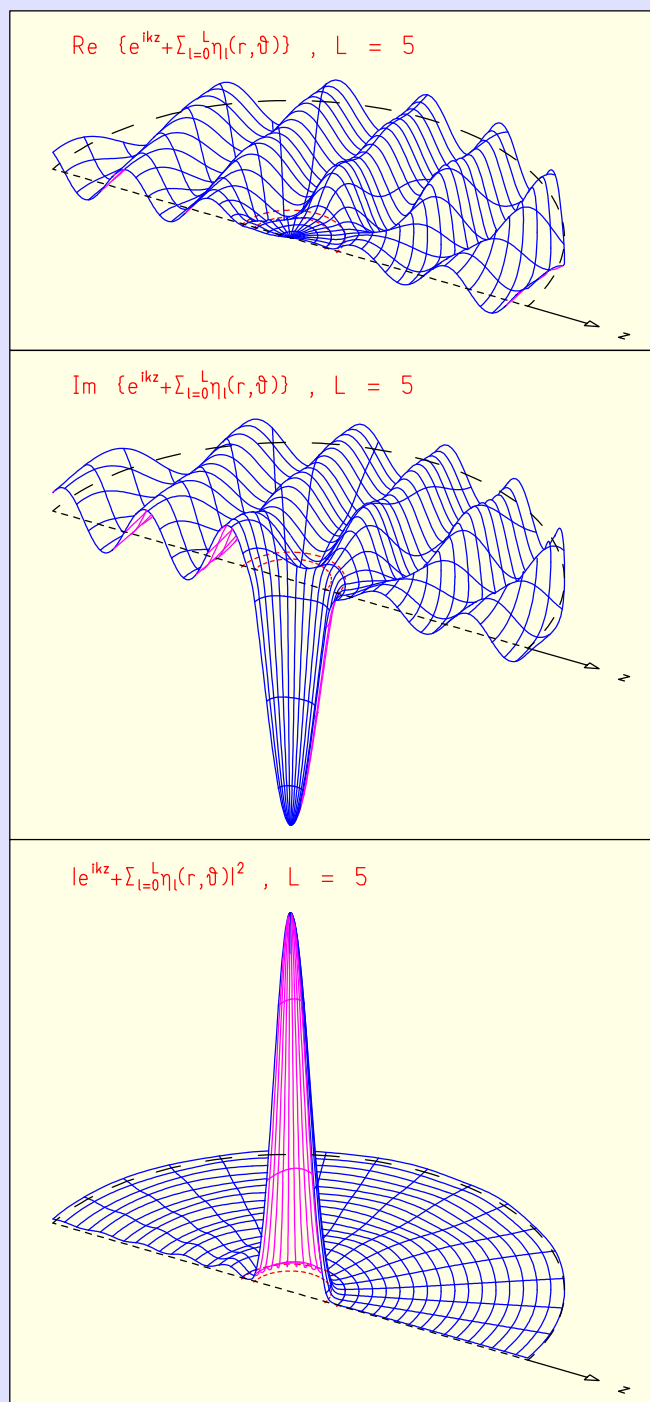


Fig. 15.19. Wave function $\varphi_{\mathbf{k}}^{(+)}$, for the first resonance in $\ell = 0$ produced by the scattering of a plane wave incident along the z direction by a repulsive potential shell.

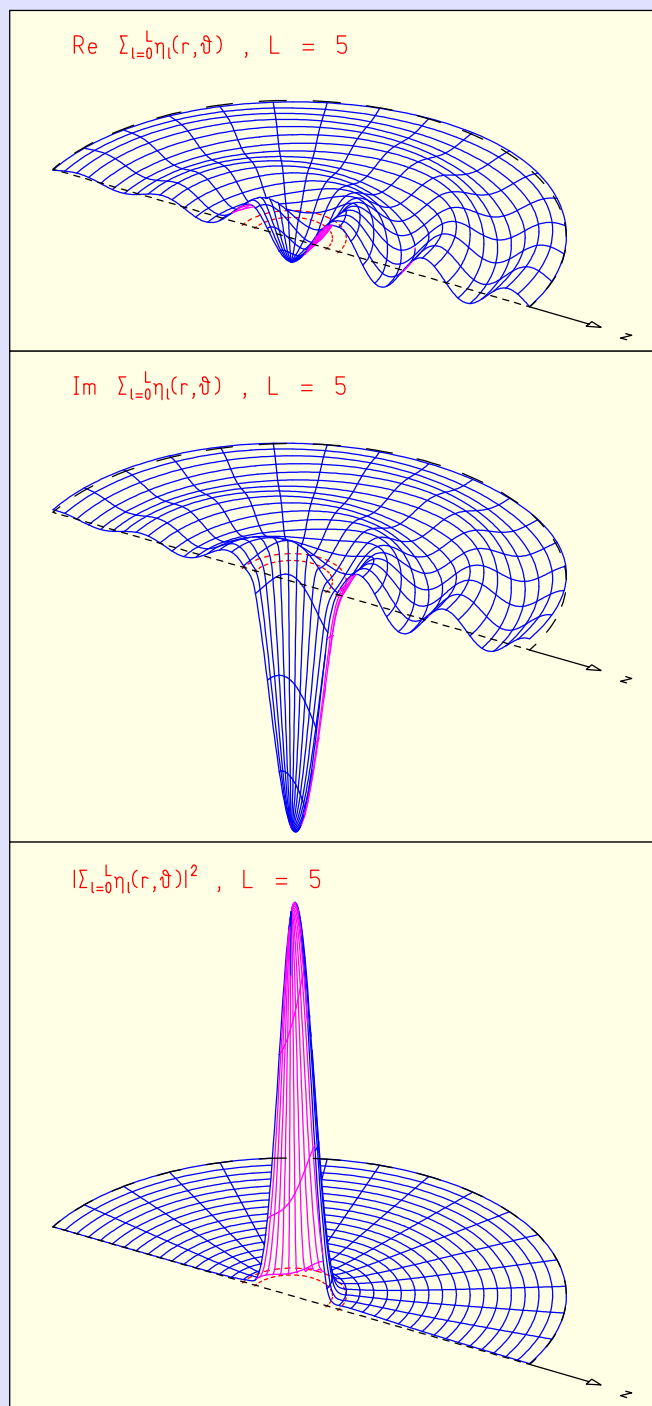


Fig. 15.20. Scattered spherical wave η_k for the first resonance in $\ell = 0$ produced by the scattering of a plane wave incident along the z direction by a repulsive potential shell.

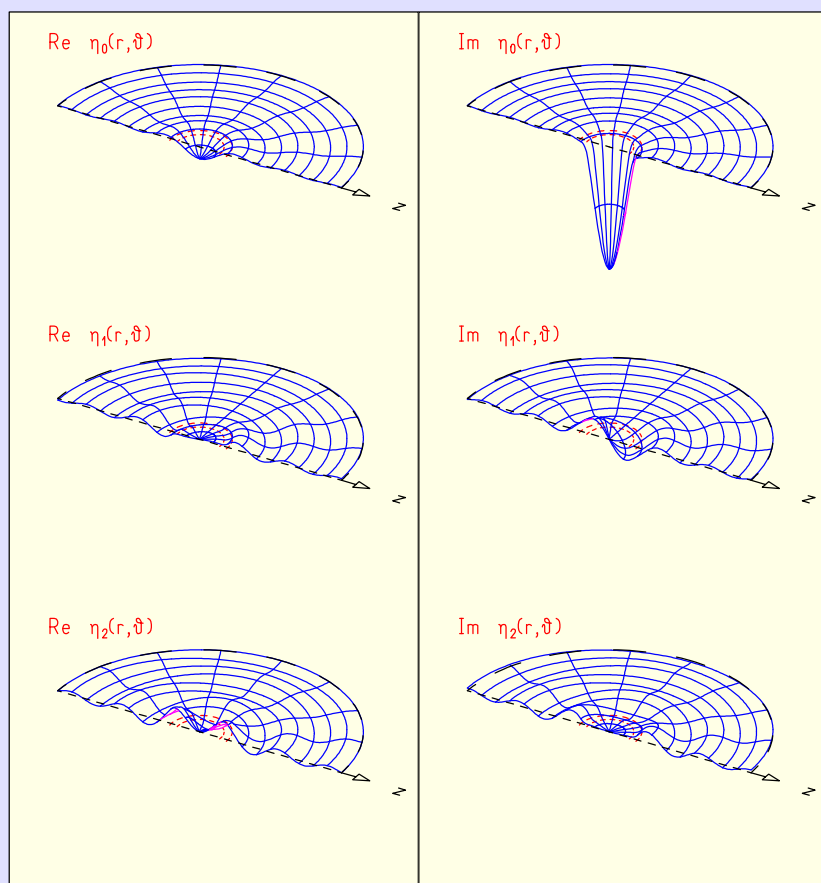


Fig. 15.21. Scattered partial waves η_ℓ for the first resonance in $\ell = 0$ produced by the scattering of a plane wave incident along the z direction by a repulsive potential shell.